J Appl Electrochem (2007) 37:1313–1319
DOI 10.1007/s10800-007-9415-0

ORIGINAL PAPER

Effect of oxidisable substrates on the photoelectrocatalytic properties of thermally grown and particulate TiO_2 layers

Josef Krýsa · Martin Zlámal · Georg Waldner

Received: 7 March 2007 / Revised: 31 August 2007 / Accepted: 1 September 2007 / Published online: 21 September 2007

Abstract The photoelectrochemical properties of titanium dioxide layers, prepared by thermal oxidation of titanium at 500–750 °C, were compared with those of layers of particulate (Degussa) P25, especially for oxidation of oxalic acid. The thermally formed oxide layers had rutile structures with a particle size of about 100 nm. Values of incident photon-to-current conversion efficiencies increased with rutile layer thickness and reached a maximum at about 1 μm. Photocurrents for particulate TiO_2 layers were about one order lower than those for thermal layers, due to the poor contact among individual particles, resulting in high electric resistance of the whole layer. The presence of oxalic acid had no effect on the photocurrent of thermal TiO_2 layers, while in the case of porous particulate layers, the photocurrent increased strongly, due to oxalate adsorption and subsequent enhanced oxidation rate with photogenerated holes. For oxalic acid concentrations $\leq 10^{-3}$ M, the photocurrent decayed due to mass transfer limitations, resulting in oxalate depletion in the porous particulate layer.

Keywords Titanium dioxide · Rutile · Degussa P25 · Thermal oxidation · Photocurrent IPCE · Open circuit potential · Oxalic acid

J. Krýsa (✉) · M. Zlámal
Department of Inorganic Technology, Institute of Chemical Technology, Prague, Technická 5, 166 28 Prague 6, Czech Republic
e-mail: Josef.Krysa@vscht.cz

G. Waldner
Functional Materials, Austrian Research Centers – GmbH – ARC, 2444 Seibersdorf, Austria

1 Introduction

Photocatalysis on semiconducting TiO_2 particles results from their absorbing photons with ultra-band gap energies and photogenerating electrons and holes. These charge carriers either recombine inside the particles or move to their surfaces, where they can react with adsorbed molecules; surface recombination is another possible loss mechanism. Positive holes may oxidize organic compounds, inducing their degradation, while electrons may reduce molecular oxygen to superoxide radical anions. Recombination of photogenerated holes and electrons is responsible for the relatively low quantum yield of photocatalytic degradation of organics.

Titanium dioxide is the most often used photocatalyst. The easiest way to prepare TiO_2 layers is by thermal oxidation of titanium [1–4] or titanium alloys [5]. Oxidation proceeds in air [1, 4] or oxygen [6] at temperatures between 500 and 800 °C. Due to good adhesion of TiO_2 to Ti substrates, such layers have very good mechanical properties. Furthermore, due to the conductivity of the substrate, a bias potential can be applied during irradiation and thus increases the rate of photocatalysis [1, 7–10].

A very important step in the preparation of oxide layers, especially for short oxidation times, is the pre-treatment prior to thermal oxidation; insufficient pre-treatment results in inhomogeneity. Firstly, the titanium is degreased, often using ethanol. The subsequent etching can then be performed either in Kroll acid (4% HF, 30% HCl) [4] or in a mixture of 2% HF and 11% HNO_3 [11] to remove passive oxide layers.

The recombination of photogenerated holes and electrons can be minimized by deposition of the catalyst layer on a conductive support and applying an external bias [12]. The special advantage of TiO_2 layers grown thermally on titanium is the support's high electronic conductivity. The

photocurrent is a measure of the rate of redox reactions occurring on the surface of the catalyst, e.g. oxidation of water or other oxidizable substances, and reduction of dissolved oxygen or of water to hydrogen.

Mintsouli et al. [13] recently reported the photoelectrochemical characterization of TiO_2 grown by thermal oxidation of Ti in air and particulate (Degussa P25) TiO_2 electrodes, which were heated at 500 and 700 °C. It was found that photocurrent depends on coatings surface area and crystallographic form. Although the thermally-grown TiO_2 electrodes produced higher photocurrent than the particulate electrodes, the efficiency of thermally-grown (700 °C) TiO_2 electrodes for oxalate photo-oxidation during bulk photoelectrolysis was comparable to that of particulate electrodes.

The main objectives of the present work were: (i) determination of the relationship between the open circuit potential and photocurrent, (ii) elucidation of the effect of oxidisable substrate (oxalic acid, 4-chlorophenol) on the photoelectrochemical response of TiO_2 films prepared by thermal oxidation of Ti at various temperatures between 500 and 750 °C and of Degussa P25 particles deposited on fluoride-doped tin oxide.

2 Experimental

2.1 Oxide film preparation

Technical purity (99.9% Ti) titanium metal plates of dimensions $50 \times 15 \times 1$ mm^3 were pre-treated by immersion in a solution containing 13% (w/w) HNO_3 and 2.5% (w/w) HF for 10 s and then rinsed with distilled water and dried at ambient temperature. The plates were then oxidised thermally in air at 500, 550, 600, 650, 700, 725 and 750 °C for 30 min. Assuming that a homogeneous compact TiO_2 layer was formed [14], that there are no nitrides and all oxygen was in the form of oxide, gravimetry can be used for thickness determination.

A procedure similar to that reported by Vinodgopal et al. [15] was used for producing particulate layers. 1 cm^3 of an aqueous suspension of Degussa P25 particles (0.5 g/dm^3) was deposited on fluoride-doped tin oxide (FTO) conducting glass substrate (F:SnO_2 (Solems, France), sheet resistivity: 10 Ω/square). After drying under laboratory conditions, the layer was heated at 300 °C for 30 min, producing a deposit of 1.0 mg TiO_2 cm^{-2} equivalent to a calculated thickness of 2.7 μm, assuming a fully dense layer.

2.2 Characterization of layers

The presence of crystalline phases was determined by X-ray diffraction using a Seifert XRD 3000 P diffractometer with Co radiation and software X'Pert Pro + High Score Plus. The surface morphology was determined by scanning electron microscopy (SEM, Hitachi S4700).

2.3 Photoelectrochemical measurements

The electrochemical cell for the photoelectrochemical measurements consisted of a working electrode (TiO_2 film on Ti), a saturated calomel reference electrode (+0.24 V vs. SHE) [16] and a Pt counter electrode. A Zeiss ST41 housing with a 45 W mercury medium pressure Heraeus lamp was used as irradiation source, monochromatized by a 365 nm interference filter. A Hamamatsu S1337-1010BQ Si photodiode was used for measuring the light intensity, which was 3 mW cm^{-2} at 365 nm for most experiments.

Reference and working electrode compartments were separated by glass frit; 0.1 M Na_2SO_4 was used as electrolyte, and a magnetic stirrer was used for mixing. Chopped light polarization curves were measured using potentiostat HEKA PG-310 controlled by a PC via the software PotPulse. The term 'chopped light' means that the incident light was chopped mechanically to produce periods of dark and light at regular intervals (e.g. 4 s) during j–E curve measurement. This allowed the determination of dark current and photocurrent in a single polarization curve. Potential was swept from –0.1 to 1.4 V (SCE) at a scan rate of 40 mV s^{-1}. Values of incident-photon-to-current conversion efficiency (IPCE) were calculated using the equation:

$$\mathrm{IPCE} = \frac{j}{FP} \tag{1}$$

where j is the photocurrent density [A cm^{-2}], F is the Faraday constant and P is incident light intensity [mol photons cm^{-2} s^{-1}].

3 Results

3.1 Layer characterization

Figure 1 (open symbols) shows thicknesses of the oxide films (d_{TiO2}) in μm, calculated from the weight gain, using 4.25 g cm^{-3} for the density of rutile [17], as a function of oxidation temperature T (°C). Regression analysis was used to define the correlation:

$$d_{TiO_2} = 1.02\mathrm{e}^{0.019\,T} \tag{2}$$

A similar dependence of thickness on heating temperature (shown as closed symbols in Fig. 1) was obtained by Palombari et al. [4] who used SEM method. The SEM

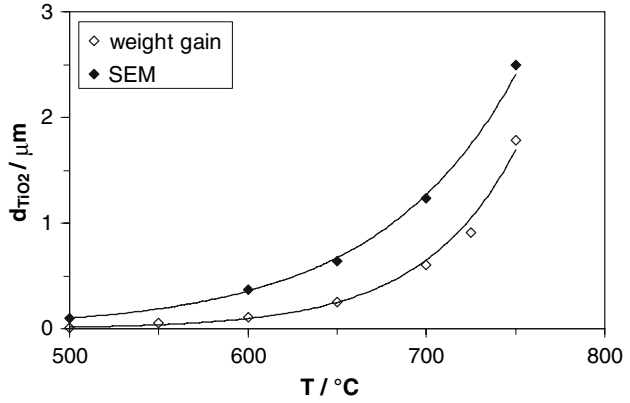

Fig. 1 Rutile TiO_2 film thickness as a function of temperature of Ti oxidation for 30 min in air. Open symbols—weight gain method; closed symbols—SEM method [4]

values of thickness are higher, due to the longer heating times (2 h), but Fig. 1 unquestionably shows that the weight gain method can be successfully used to determine layer thickness of thermal TiO_2 films.

X-ray diffraction patterns for Ti plates without treatment and those oxidized for 30 min at temperatures 500–750 °C are shown in Fig. 2. Line positions for titanium, rutile and anatase crystalline structure are marked Ti, R and A, respectively. For oxidation temperatures greater than 550 °C, peaks corresponding to rutile were clearly evident, while those for anatase were absent. It is apparent that with increasing oxidation temperature, the intensities of rutile lines increased, which corresponds to increasing oxide layer thickness.

Palombari et al. [4] reported the presence of rutile, whereas Mintsouli et al. [13] found anatase; neither reported the diffraction patterns of Ti sample heated at 500 °C. In the present study, anatase lines were absent, but the indication of the strongest rutile line ($2\Theta = 27.45°$, 110) was evident, corroborating the findings of Palombari et al. [4]. At 650 °C, Fig. 2 shows broadening and shifting of all Ti lines, probably due to the presence of oxygen in the Ti lattice, whereas at 750 °C, the Ti lines were not apparent, due to the greater TiO_2 thickness.

Figure 3 shows the similar morphologies of Ti plates prior to, and after, thermal oxidation at 700 °C; the rough surface due to oxide formation was visible only at high resolution. The photomicrograph in Fig. 3a shows crystallite sizes of ca. 100–150 nm, which is very similar to the 100 nm size of rutile crystals calculated using Scherrer's equation ($2\Theta = 27.45°$). By contrast, SEM images of particulate P25 layers show aggregates of size ca. 5 µm, while anatase crystal sizes were ca. 30 nm [18].

3.2 Photoelectrochemical properties

Figure 4 shows the effects of irradiation on the time dependence of open circuit potentials (E_{oc}) of a Ti/TiO_2 electrode in 0.1 M Na_2SO_4 at neutral pH. During the dark period, Ti/TiO_2 electrodes had potentials of ca. –0.1 V (SCE), which decreased upon illumination by 0.05–0.3 V, depending on the pre-treatment temperature.

This could be attributed to photogenerated holes reacting rapidly with water on the surface to hydroxyl radicals. As the reaction rate of photogenerated electrons is slower, there was a net accumulation of electrons causing partial reduction of Ti^{IV} to Ti^{III} and the electrode potential to decrease. Even an untreated Ti substrate with a thin passive oxide film formed at room temperature in air exhibited a negative shift of E_{oc}, which increased with increasing

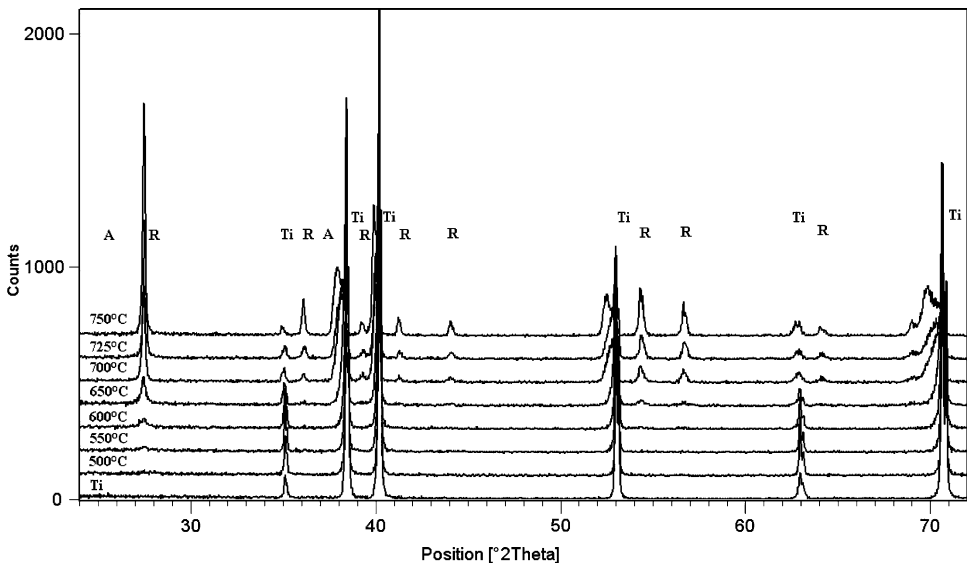

Fig. 2 X-ray diffraction patterns of non-treated Ti plate and Ti plate heated at 500–750 °C for 30 min in air

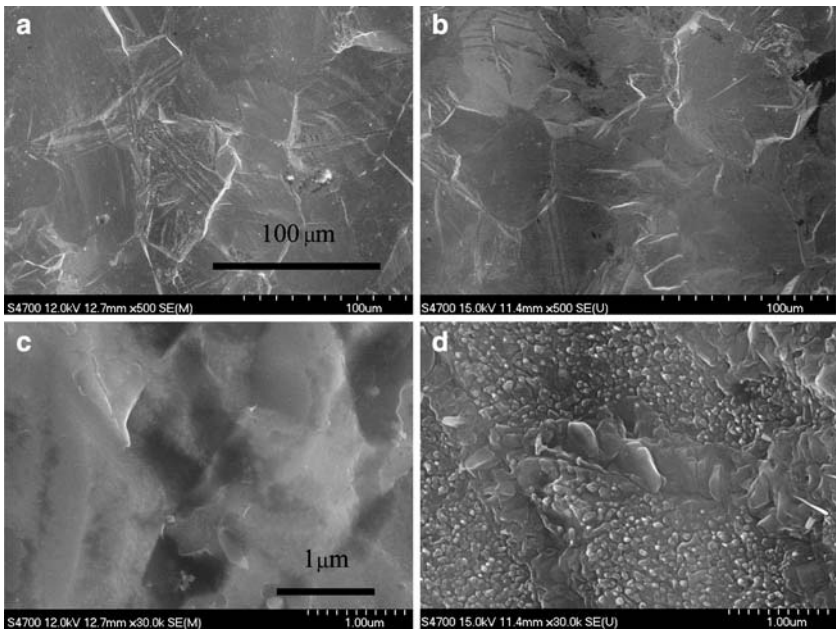

Fig. 3 Morphology of Ti plates (SEM), (**a**, **c**) without treatment, (**b**, **d**) heated at 700 °C for 30 min in air

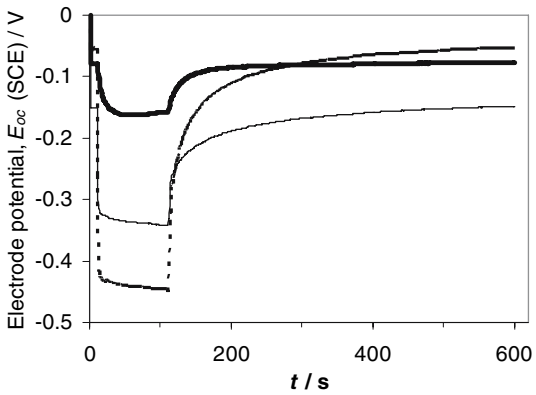

Fig. 4 Open circuit potential of Ti/TiO_2 in 0.1 M Na_2SO_4 (neutral pH) as a function of irradiation time. Bold line—Ti plate without treatment, solid line—Ti plate heated at 600 °C, broken line—Ti plate heated at 700 °C for 30 min in air

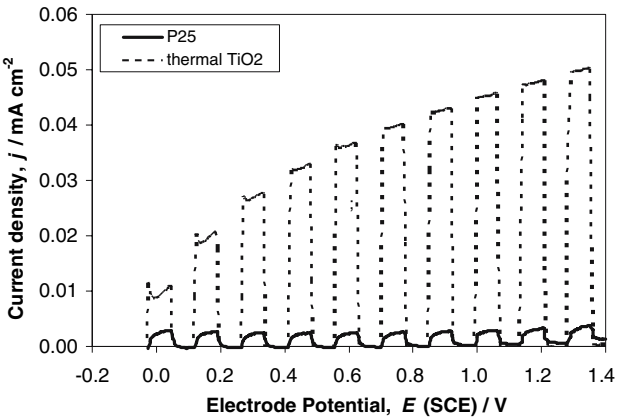

Fig. 5 Chopped light polarization curve for two types of TiO_2 layer in 0.1 M Na_2SO_4; (neutral pH), 40 mV s^{-1}; solid line—particulate P25 (0.5 mg cm^{-2}), broken line—thermal oxidation at 700 °C for 30 min in air

temperature of prior oxidation. This can be explained by the increasing oxide layer thickness, resulting in greater absorption of UV photons and hence increasing concentration of trapped photogenerated electrons.

Figure 5 shows the chopped light polarization behaviour in 0.1 M Na_2SO_4 for a thermally-grown TiO_2 layer formed at 700 °C, compared with that for a porous P25 layer. It is apparent that the current response was fast, due to rapid migration of photogenerated charge carriers in the thermal oxide layer. Photocurrents for thermal TiO_2 layers were greater than that for particulate layers. This was due to the poor contact between individual particles in the layer, resulting in high electric resistance of the whole layer, as reported previously [2, 13]. The high resistance was also responsible for rather slow photocurrent response to light in the case of porous P25 layers.

Chopped light polarization curves were measured for thermally grown TiO_2 layers produced by oxidation of Ti at 500–750 °C. Photocurrents at 0.8 V (SCE) were determined as a function of layer thickness and values of incident photon-to-current conversion efficiencies (IPCE) were calculated using Eq. 1. Data in Table 1 and Fig. 6 indicate that IPCEs increased, and open circuit potentials E_{oc} decreased, with increasing oxidation temperature/layer thickness, up to a maximum value of 0.66 at 0.91 μm, corresponding to 725 °C, above which IPCEs decreased to 0.31 at 1.78 μm. This decrease may have been due to that part of the layer closer to the Ti substrate suffering severe attenuation of the photon flux, due to absorption in the outer part of the layer; hence, the inner layer may have behaved as a resistance barrier to electron migration from

Table 1 TiO_2 layer thickness, open circuit potentials and IPCE at 0.8 V (SCE) for Ti plates heated for 30 min at various temperatures

T (°C)	d (μm)	E_{oc} (SCE) (V)	IPCE
No	Treatment	–0.158	0.03
500	0.010	–0.339	0.20
550	0.05	–0.334	0.19
600	0.11	–0.341	0.32
650	0.25	–0.406	0.54
700	0.60	–0.451	0.61
725	0.91	–0.473	0.66
750	1.78	–0.445	0.31

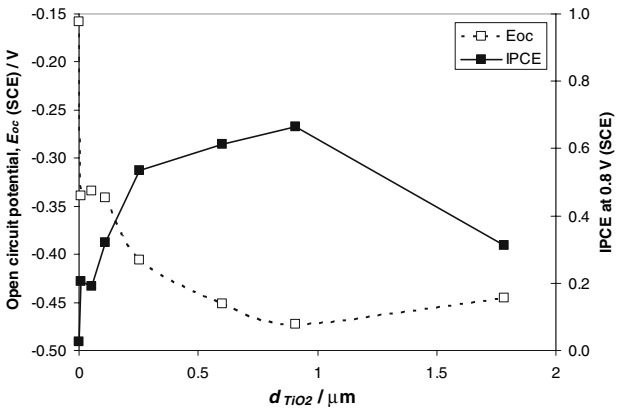

Fig. 6 Open circuit potential and IPCEs at 0.8 V (SCE) of Ti/TiO_2 in 0.1 M Na_2SO_4 (neutral pH) as a function of TiO_2 layer thickness

the irradiated outer part of the TiO_2 layer to the Ti substrate. The increase of IPCE with increasing temperature of Ti oxidation from 500 to 700 °C is similar as that reported by Mintsouli et al. [13], although they did not report corresponding TiO_2 layer thicknesses.

3.3 Effect of oxidisable organic substrates

Figure 7 shows the effect of electrode potential on the photocurrent response to chopped light of a TiO_2 layer grown by thermal oxidation of Ti at 725 °C, and in presence of 1 mM oxalic acid (pH = 2.5) and 4-chlorophenol, which have different adsorption properties. This oxide layer was chosen as it produced the highest value of IPCE in supporting electrolyte alone; addition of either oxalate or 4-CP decreased that photocurrent.

Addition of 4-chlorophenol had no effect on the magnitude of the photocurrent from particulate P25 layers. For a compact rutile film, dark current was negligible up to potential 1.4 V (SCE), but for the porous P25 layer, a current onset was evident at ca. 0.6 V (SCE) (not shown here). A similar onset value (0.8 V (SCE)) was observed by

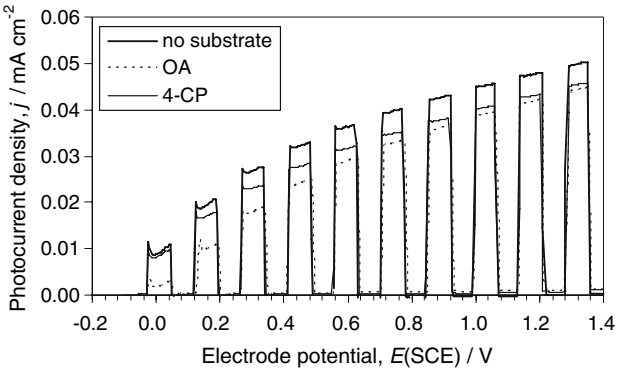

Fig. 7 Effect of 10^{-3} M oxalic acid (pH = 2.5) and 4-chlorophenol on the potential dependence of photocurrent for a TiO_2 layer grown by aerial oxidation of Ti at 725 °C for 30 min; 0.1 M Na_2SO_4; 40 mV^{-1}

Wang et al. [19], who studied the electrochemical oxidation of 4-chlorophenol on a nickel–antimony doped tin oxide electrode. This suggests that due to the porous structure of P25 layer, 4-chlorophenol had access to the conductive SnO_2 layer and thus oxidation started at lower potentials than on compact TiO_2 layers.

In contrast to thermal layers, in the case of particulate P25 layers, photocurrents increased significantly in the presence of oxalic acid about 5–35 times, depending on its concentration (see Fig. 5 in [20]). As already mentioned by Byrne et al. [21] the huge increase in photocurrent cannot be due to the current doubling alone. The different behaviour of the two TiO_2 layers can be explained by the porous structure of the particular layer, resulting in high surface area. Thus, a significant amount of oxalate ions was adsorbed and this helped to decrease recombination rates, by decreasing hole concentrations due to their fast reaction with oxalate; hence IPCEs increased.

Figure 8a and b show the time dependence of the photocurrent at 0.8 V (SCE) for particulate P25 layers in 5×10^{-2} M, 10^{-3} M and 10^{-4} M oxalic acid. For the highest concentration, the photocurrent was constant during whole irradiation period, whereas in 10^{-3} M oxalic acid, the initial photocurrent was slightly lower than at the higher concentration and decreased further with irradiation time, but reached a steady state after ca. 100 s. When the irradiation was stopped for about 50 s and restarted again, the same photocurrent-time behaviour resulted.

In the case of 10^{-4} M oxalic acid, the initial photocurrent was much lower, due to the lower concentration of adsorbed species, and decreased sharply with irradiation time to a steady state photocurrent density of ca. 10^{-5} A cm^{-2}, only three times greater than in 0.1 M Na_2SO_4 alone (Fig. 5). Interruption of irradiation for short times resulted in an increase of initial photocurrent, but for full recovery

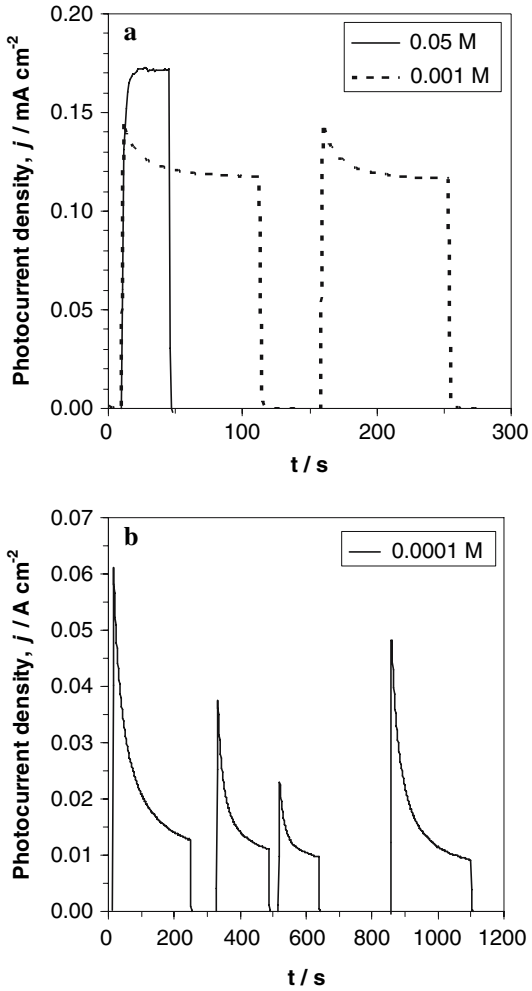

Fig. 8 Photocurrent density—time behaviour of P25 particulate layer at 0.8 V (SCE) for oxalic acid concentrations. (**a**)—5×10^{-2} and 10^{-3} M, (**b**)—10^{-4} M

of initial adsorption densities of oxalate ions, much longer times without irradiation were necessary.

Table 2 lists values of initial photocurrent density ($i_{ph,i}$), ratio of steady state and initial photocurrent densities ($i_{ph,st}/i_{ph,i}$) from data in Fig. 8, and those reported by Byrne et al. [21], who observed similar photocurrent decay on P25 films in the presence of 10^{-3}–10^{-2} M oxalic acid. Adsorption isotherms [22] showed increased adsorption densities of oxalic acid up to equilibrium concentrations of only 5×10^{-3} M, above which they reached a plateau value. Table 2 gives oxalate ion adsorption densities on P25 TiO_2 particles [22] for concentrations used in these experiments, showing that the value of the initial photocurrent was determined by the adsorption density rather than bulk concentration of oxalate ions. For example, when that concentration was decreased from 5×10^{-2} M to 10^{-3} M, the photocurrent decreased to only 85% of its value at 0.05 M and adsorption density decreased to 70% of its value at 5×10^{-2} M.

Table 2 Photocurrent densities and adsorption density of oxalic acid at various concentrations

c_{OA} (M)	$j_{ph,in}$ (mA cm^{-2})	$j_{ph,st}$ (mA cm^{-2})	$j_{ph,st}/j_{ph,in}$	$j_{ph,st}/j_{ph,in}$ [20]	n_{OA} (μmol g^{-1}) [21]
0.05	0.17	0.17	1	–	14
0.01	–	–	–	0.6	14
0.001	0.145	0.12	0.83	0.35	9
0.0001	0.06	0.01	0.16	–	–

A possible explanation of the photocurrent—time behaviour can be proposed as follows. Prior to illumination, due to strong adsorption, oxalate ions penetrated the whole of the TiO_2 particulate layer. When irradiation started, adsorbed oxalate ions were oxidised rapidly by holes at the porous TiO_2/solution interface and photogenerated electrons diffused and migrated through the layer to the Ti contact, producing the large initial photocurrent. At concentration 5×10^{-2} M, the photo-oxidised oxalate ions are quickly replaced by pore diffusion, so the photocurrent did not decay. At low bulk concentrations, the oxalate concentration in the electrolyte within the film was depleted, especially in the depth of the pores toward the Ti contact. Photogenerated electrons migrate through the particulate film to reach the contact, passing through an oxalate-depleted region, with a high concentration of surface trapped holes. Hence, a significant proportion of photogenerated electrons are lost by recombination, resulting in the photocurrent decay with time.

4 Conclusions

Oxide layers prepared by thermal oxidation of Ti in air at 500–750 °C have rutile structure with particle sizes of about 100 nm. Values of IPCE increased with layer thickness and reached a maximum at 1 μm. The open circuit potential decreased as the IPCE increased with increasing film thickness, due to greater photon absorption and faster hole than electron consumption reaction rates.

Addition of either oxalic acid or 4-chlorophenol had no effect on photocurrents of thermal TiO_2 layers, whereas for porous particulate layers, adsorption of oxalate ions and its subsequent enhanced reaction rate with photogenerated holes increased photocurrent strongly. For particulate TiO_2 layers and oxalic acid concentrations <0.001 M, the photoelectrochemical oxidation was mass transfer controlled, causing oxalate depletion through the porous layer so that photocurrents decayed with time.

Acknowledgement The authors thank the Ministry of Education, Youth and Sport of the Czech Republic for financial support (project No. 1M057 and MSM 6046137301).

References

1. Butterfield IM, Christensen PA, Hamnett A, Shaw KE, Walker GM, Walker SA (1997) J Appl Electrochem 27:385
2. Waldner G, Krýsa J (2005) Electrochim Acta 50:4498
3. Camara OR, De Pauli CP, Vaschetto ME, Retamal B, Aquirre MJ, Zagal JH, Biaggio SR (1995) J Appl Electrochem 25:247
4. Palombari R, Ranchella M, Rol C, Sebastiani GV (2002) Solar Energy Mat Solar Cells 71:359
5. Kudo A, Steinberg M, Bard AJ, Campion A, Fox MA, Mallouk TE, Webber SE, White JM (1990) J Electrochem Soc 137:3846
6. Waldner G, Pourmodjib M, Bauer R, Neumann-Spallart M (2003) Chemosphere 50:989
7. Candal RJ, Zeltner WA, Anderson MA (2000) Environ Sci Technol 34:3443
8. Fernandez P, Malato S, Enea O (1999) Catal Today 54:329
9. Krýsa J, Jirkovský J (2002) J Appl Electrochem 30:591
10. Waldner G, Brüger A, Gaikwad NS, Neumann-Spallart M (2007) Chemosphere 67:779
11. Waldner G (2003) Heterogeneous photocatalytic and photo-electrocatalytic purification of water. Dissertation, Technical University Wien
12. Rajeshwar K (1995) J Appl Electrochem 25:1067
13. Mintsouli I, Philippidis N, Poulios I, Sotiropoulos S (2006) J Appl Electrochem 36:463
14. Finklea HO (1988) Stud Phys Theor Chem 55:43
15. Vinodgopal K, Stafford U, Gray KA, Kamat PV (1994) J Phys Chem 98:6797
16. Ives DJ, Janz GJ (1961) Reference electrodes. Academic, New York
17. http://www.webmineral.com/data/Rutile.shtml
18. Krýsa K, Keppert M, Waldner G, Jirkovský J (2005) Electrochim Acta 50:5255
19. Wang YH, Chan KY, Li XY, So SK (2006) Chemosphere 65:1087
20. Waldner G, Krýsa J, Jirkovský J, Grabner G (2003) Int J Photoenergy 5:115
21. Byrne JA, Eggins BR (1998) J Electroanal Chem 457:61
22. Robert D, Weber JV (2000) Adsorption 6:175